NANO LETTERS

Letter

pubs.acs.org/NanoLett

In Situ Generation of Surface Plasmon Polaritons Using a Near-Infrared Laser Diode

D. Costantini,[†] L. Greusard,[‡] A. Bousseksou,[†] R. Rungsawang,[‡] T. P. Zhang,[§] S. Callard,[§] J. Decobert,[∥] F. Lelarge,[∥] G.-H. Duan,[∥] Y. De Wilde,*[,‡] and R. Colombelli*[,†]

[†]Institut d'Electronique Fondamentale, Univ. Paris Sud, CNRS UMR8622, 91405 Orsay, France

[‡]Institut Langevin, ESPCI ParisTech, CNRS, 1, rue Jussieu, 75238 Paris Cedex 05, France

[§]Université de Lyon, Institut des Nanotechnologies de Lyon, UMR 5270, CNRS, Ecole Centrale de Lyon, Avenue Guy de Collongue, F-69134 Cedex, France

[∥]III-V Lab, Joint lab of 'Alcatel-Lucent Bell Laboratories France', 'Thales Research and Technology' and 'CEA Leti', route de Nozay, 91461 Marcoussis Cedex, France

ABSTRACT: We demonstrate a semiconductor laser-based approach which enables plasmonic active devices in the telecom wavelength range. We show that optimized laser structures based on tensile-strained InGaAlAs quantum wells—coupled to integrated metallic patternings—enable surface plasmon generation in an electrically driven compact device. Experimental evidence of surface plasmon generation is obtained with the slit-doublet experiment in the near-field, using near-field scanning optical microscopy measurements.

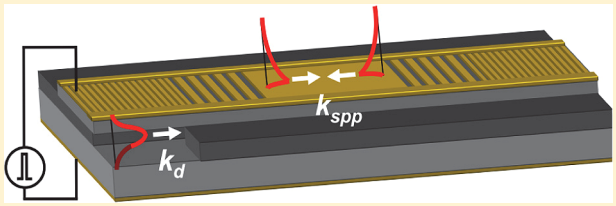

KEYWORDS: *Plasmonics, surface-plasmon generation/amplification, diode laser, quantum wells, distributed-feedback lasers*

Several surface plasmon polariton (SPP) passive components have been demonstrated to date, showing attractive performances for extreme light confinement and high bandwidth modulation.[1,2] On the other hand, the lack of a viable technology to compensate for the large optical losses, typical of SPPs, limits practical applications. Recently, efforts have been devoted to the development of active SPP devices, both for generation/amplification,[3,4] coupling,[5,6] and stimulated emission.[7−9] The development of plasmonic active devices at telecom wavelengths (λ = 1.3−1.55 μm) is relevant because of the compatibility with current commercial platforms based on fiber optics for communications. Recent work in ref 10 proposed the use of optically pumped lead sulfide (PbS) quantum dots to partially compensate SPP propagation losses at λ = 1.55 μm. Our goal is to develop a semiconductor-based approach enabling plasmonic electrically pumped active devices in the telecom wavelength range.

A basic design of integrated SPP generator was initially demonstrated at long mid-infrared wavelengths (λ ∼7.5 μm) by coupling a semiconductor quantum cascade laser (QCL) with a plasmonic metallic waveguide.[11] This architecture relies on an "end-fire" coupling in which the two waveguides are contiguous. Its coupling efficiency depends on the relative positions of the QCL and metallic waveguides, and on the geometrical overlap between the dielectric laser mode and the SPP mode. This scheme was recently implemented at telecom wavelengths by Kim et al.[12]

In this paper, we demonstrate an alternative elegant strategy for a compact and integrated SPP generator, which operates under electrical injection and at telecom wavelengths. A laser cavity mode is coupled to a propagating SPP mode in a metal−air interface *via* metallic grating couplers. The demonstration is inspired by the slit-doublet experiment revisited in the near field.[13]

Design. SPPs are transverse magnetic (TM) polarized surface waves. Their generation with devices based on planar architectures is possible only if light with the same polarization is produced. This requirement is satisfied at λ = 1.3−1.55 μm using laser diodes with an active region (AR) based on tensile-strained InGaAlAs semiconductor quantum wells.[14] This semiconductor gain medium suits device applications, since it is compatible with electrical injection. On the other hand, a p-doped semiconductor top-cladding is necessary for the correct operation of the diode junction. The thickness of this layer is a crucial device parameter, since it affects simultaneously—but in opposite directions—the coupling efficiency between the laser mode and the SPP wave, and the waveguide laser losses induced by the proximity of the top metal contact. In ref 15, we have developed a structure which represents an optimal trade-off between coupling efficiency and optical losses. We employ that structure in this work (see Table I in ref 15). The total cladding thickness is 450 nm, and the AR is composed of nine quantum wells.

Received: May 30, 2012
Revised: August 19, 2012
Published: August 27, 2012

   dx.doi.org/10.1021/nl302040e | *Nano Lett.* 2012, 12, 4693−4697

The telecom wavelength plasmonic devices presented in this work are composed of three key features: the laser cavity, the grating couplers, and the plasmonic waveguide. These features are integrated in a single device which is electrically driven. Our work is inspired by the analogous demonstration that we have recently reported at mid-infrared wavelengths using QCLs operating at 7.5 μm.[16]

Integrated SPP generation is obtained by coupling a semiconductor laser source with a plasmonic waveguide *via* a judiciously designed coupler grating section, which compensates for the momentum difference between the SPP and the waveguided mode. The coupler is compact, since it is a few micrometers long, and it can be easily integrated. A single metal deposition step is employed, which simultaneously forms the passive plasmonic waveguide, the coupler, and the top contact of the diode laser. No alignment step between laser and plasmonic waveguide is necessary, thus considerably simplifying the technology. The diode laser top contact (made of gold) is periodically patterned to obtain single-mode spectral operation according to the distributed feedback (DFB) laser cavity concept.[17]

The schematic top view in Figure 1a shows the three key features of the device. The laser cavity and the two coupling

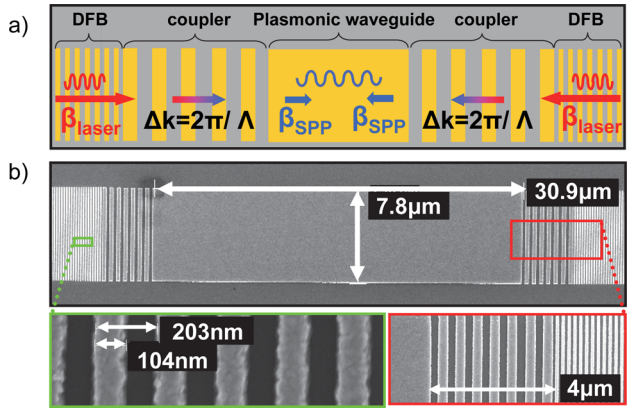

Figure 1. (a) Schematics of the top metal patterning which defines the three basic device components: first-order grating for the DFB cavity, the coupler grating, and the passive plasmonic waveguide. The configuration is symmetric in order to inject SPP from both sides of the passive waveguide (counter-propagation configuration). The red and blue arrows show the propagation direction and are proportional to the wavevector of the DFB mode (β_{laser}) and of the SPP (β_{SPP}), respectively. The bicolored arrows are proportional to the momentum provided by the couplers to match DFB and SPP modes ($\Delta k = 2\pi/\Lambda = \beta_{laser} - \beta_{SPP}$). (b) SEM image of the top metal patterning with close-ups of the coupler and of the DFB grating. The surface is patterned using electron-beam lithography, followed by lift-off of a 70 nm thick metal layer (3 nm Ti, 67 nm Au) deposited with electron-beam evaporation.

gratings are fabricated one in front of the other, separated by a passive, unpatterned *plasmonic* waveguide 30 μm long. The metal thickness is 70 nm. SPPs are injected into the waveguide with opposite wavevectors. The consequence of the counter-propagation is the formation of a plasmonic standing wave.

A necessary step has been an in-depth numerical electromagnetic analysis which is reported in ref 18. We have maximized the coupling efficiency of the system—by optimizing the grating coupler parameters—up to a maximum value of more than 20%. Such a value can be obtained within a reasonably large range of geometrical parameters and of input wavelengths, a factor which simplifies the device fabrication.

Fabrication. The devices were processed into 9 μm wide, 450 nm deep mesa ridges. The surface was first patterned with metal using electron-beam lithography followed by lift-off (Figure 1b). The different motifs define the three necessary device components: the first-order Bragg grating for the DFB cavity; the grating couplers; and a central, passive plasmonic waveguide. The DFB cavity is a first-order Bragg grating with ~50% filling factor. Figure 2a shows the emitted spectra of

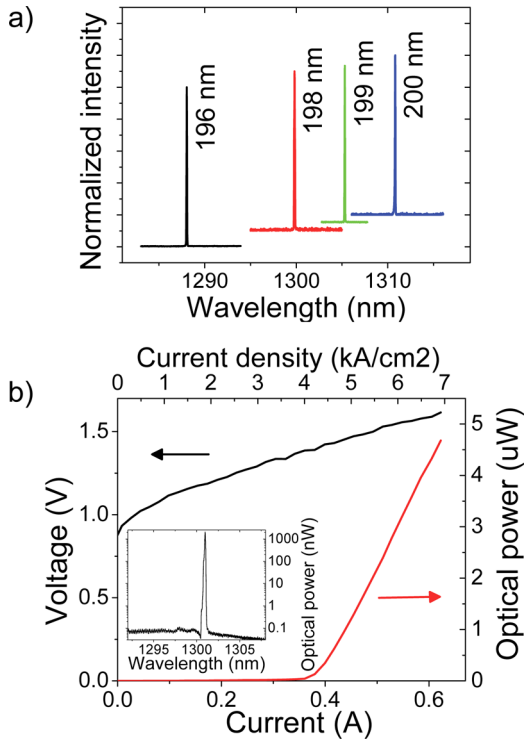

Figure 2. (a) Single mode spectra of DFB lasers with different grating periods (196, 198, 199, and 200 nm). The spectra are measured at room temperature (RT) in the pulsed regime with an optical spectrum analyzer. (b) LIV characterizations at RT in the pulsed regime (1% duty cycle) of a typical device with Λ = 198 nm. The inset shows the spectrally single mode emission collected from the device facet at an injection current of 500 mA. The side mode suppression ratio (SMSR) is more than 40 dB, and the full width at half-maximum (fwhm) is ~12 MHz (0.07 nm). Typical commercial dielectric DFB lasers exhibit a fwhm of ~1−2 MHz and threshold current densities of the order of 1 kA cm^{-2} or less.

several laser cavities with different grating periods Λ = 196-198-199-200 nm. Single mode emission which correctly tunes with the grating period is obtained. The laser mode has an optimal transverse shape: near-field scanning optical microscopy (NSOM) measurements show a single lobe confined at the center of the ridge waveguide (data not shown[19]). In fact, the results of finite element simulations confirm that the transverse mode with one lobe exhibits lower losses than higher order modes which overlap with the lateral metallic contacts on the ridge sides.

The lasers generate standing electromagnetic waves of frequency $\upsilon_{laser} = c/\lambda$ with a momentum $\beta_{laser} = 2\pi n_{eff}/\lambda = \pi/\Lambda$, where n_{eff} is the effective index of the lasing mode, λ is the free-space wavelength, and c is the speed of light in vacuum. The passive plasmonic waveguide is a strip of length L_{strip} = 30

dx.doi.org/10.1021/nl302040e | *Nano Lett.* 2012, 12, 4693−4697

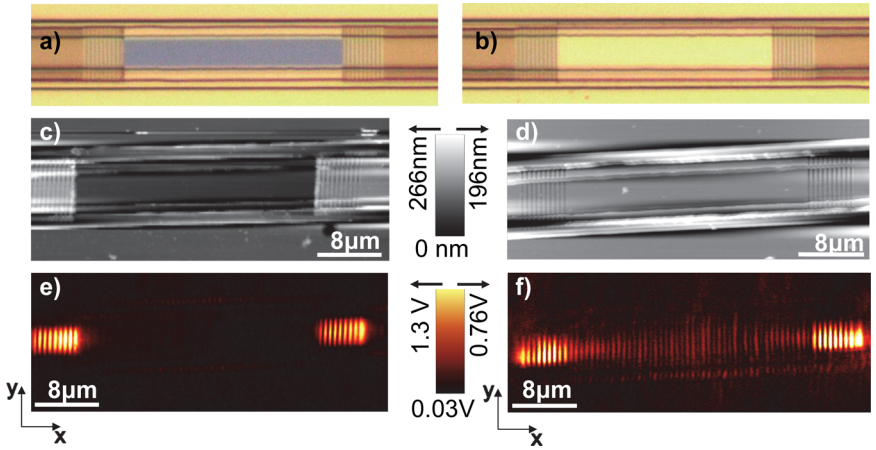

Figure 3. (a, b) Optical microscope image of a reference device (no passive metallic waveguide) and a SPP device. (c) Topographic image on the reference device (subtraction filter applied). (d) Topographic image on the SPP device (subtraction filter applied). (e, f) Near-field optical image on the reference (panel e) and SPP (panel f) device. The near-field optical signal is acquired *simultaneously* with the topography. Both devices are measured at room temperature in pulsed mode (duty cycle = 10%) at an injected current of 800 mA. The near-field optical image on the SPP device clearly shows the presence of the plasmonic interference pattern on the passive metallic waveguide, while no similar signal is visible on the reference one. A careful analysis of panel e reveals interference fringes on the ridge sides between the two couplers. These oscillations stem from SPPs propagating on the lateral gold contacts used for the current injection. This subtle observation further strengthens the result.

μm that is long enough to contain several SPP interference fringes (we estimate ~45 fringes). This ensures that a relatively wide zone will be free from stray radiation originating from the grating couplers and lead to a clear near-field detection of propagating SPPs.

The momentum of the SPPs traveling on the metal waveguide is $\beta_{SPP} = 2\pi/\lambda_{SPP} \approx 2\pi/\lambda$.

The periodicity of the coupler grating, Λ_C, is chosen to compensate the momentum difference between SPP and laser modes: $2\pi/\Lambda_C = \beta_{laser} - \beta_{SPP}$. We employed Λ_C = 580 nm and a duty cycle of 55%. Grating couplers with 7 and 10 slits were fabricated.

Figure 2b shows the room-temperature (RT) electrical characterization and the optical emission of a 1 mm long device containing the laser cavity, the grating couplers, and the plasmonic waveguide. The laser threshold current density is 4.5 kA/cm^2, and the emission is collected from the facet with a cleaved multimode fiber. The emission spectrum (Figure 2b, inset) shows single mode operation at $\lambda \approx 1300$ nm.

Near-Field Measurements and Data Interpretation. The unambiguous proof of the SPP presence and propagation on the device is provided by near-field scanning optical microscopy (NSOM). We have investigated the EM near-field distribution on the device area above the passive waveguide and the couplers. The near-field maps are collected using a commercial NSOM (WITec GmbH alpha300S) which we have adapted to near-infrared frequencies.

Our NSOM uses a silicon cantilever-based square hollow pyramid probe metalized with aluminum,[20] with a nanoaperture at its apex (diameter ~100 nm). The cantilever and the pyramid lateral facets act as a screen allowing light transmission only through the nanoaperture. The detection is performed with an InGaAs detector. To our knowledge, this is the first time that a NSOM with hollow pyramid is employed at telecom wavelengths. Note that a similar setup has been used to investigate the propagation of SPPs at short, visible wavelengths.[21,22]

The sample stage is translated during the scans using piezoelectric translators, while the tip is maintained at a fixed position. The tip−sample distance control relies on the classical beam-deflection principle using a 980 nm laser. The beam is focused through a microscope objective onto the surface of the cantilever, 100 μm away from the pyramid. A dichroic mirror sends the reflected laser into a segmented photodiode which measures the cantilever deflection.

The optical signal transmitted through the nanoaperture is collected by the same objective and focused on a multimode fiber connected to a thermoelectrically cooled InGaAs detector. The fiber itself acts as a confocal pinhole which is optically conjugated with the nanoaperture in the hollow pyramid. The current injected in the device is modulated; hence, the collected signal is demodulated at this same frequency. Near-field (xy) images of the SPPs at the device surface are obtained when scanning the device laterally with the apex of the hollow pyramid permanently in contact with the surface. Our NSOM allows us also to perform scans in a plane perpendicular to the device surface to record (xz) cross sections of the SPP field distribution. This type of measurement provides useful information on the SPP confinement and extension above the surface.

Identical measurements have been performed on SPP devices and on reference devices (i.e., devices—processed simultaneously from the same wafer—where the passive metallic waveguide is missing). Parts a and b of Figure 3 show the optical microscope images of a reference and SPP device, respectively. The topographic signal for both devices—collected *simultaneously* with the near-field one—is shown in Figure 3c and d.

Finally, Figure 3e and f shows the near-field images. Plasmonic interference fringes are clearly visible on the passive metallic waveguide between the two couplers in the SPP device only, while no analogous fringes can be observed on the *reference* device, since SPPs do not exist at the interface between air and a dielectric. The fringes stem from counter-propagating SPP waves traveling on the surface of the metallic strip, with opposite wave vectors $+\beta_{SPP}$ and $-\beta_{SPP}$. Their presence proves that SPPs are generated and launched into the passive metallic waveguide. The couplers simultaneously inject SPPs into the

dx.doi.org/10.1021/nl302040e | *Nano Lett.* 2012, 12, 4693−4697

passive waveguide[23] and diffract part of the light from the laser cavity into free space, as witnessed by the bright spots observed above the coupler areas. The NSOM measurements do not allow us to experimentally gauge the coupling efficiency, but numerical simulations[18] place an upper limit at ~24%.

We have performed 2D finite element electromagnetic numerical simulations[24] of the device. The 2D character of the simulation reduces the computational load and allows one to take into account the reduced thickness of the metallic layers (70 nm) and at the same time the considerable length of the full structure (more than 50 μm). Figure 4 (red line) shows a

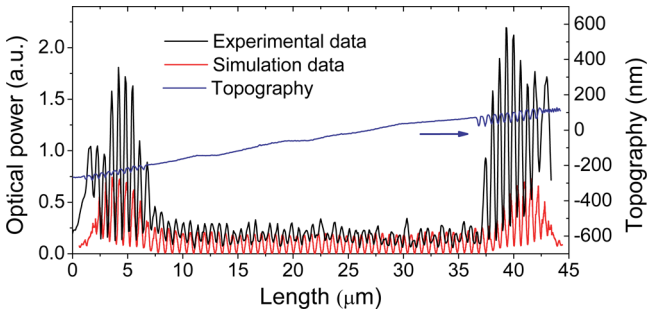

Figure 4. Intensity of the near-field optical signal at the device top surface compared with simulations. The measured data (black curve) correspond to a 1D cross section taken from Figure 3f. The numerical simulation (red curve) is a 1D cross section of the squared modulus of the electric field taken 10 nm above the device surface. The topographic measured signal (raw data, green curve) allows one to correlate the EM near field with the top metallization. The slight slope of the topography corresponds to an angle of ~0.5°, and it does not affect the optical measurements.

longitudinal cross section—taken at 10 nm above the device surface—of the electric field squared modulus obtained from the simulation. The agreement with the experimental NF signal (black line) taken from Figure 3f is excellent, in terms of SPP wavelength and global trend of the signal. The relatively larger signal on the coupler zones with respect to the simulation possibly stems from higher light scattering, due to fabrication nonidealities.

The numerical simulation also provides the extension of the interferential plasmonic pattern in the $x-z$ plane. Figure 5a shows the axis definition and a schematic view of the simulation domain. The result of the simulation (Figure 5b) reveals that the full interference pattern is composed of a pure SPP component, highly confined up to ~800 nm close to the metallic surface, and a quasi-cylindrical wave component.[23] The latter waves originate from the couplers and counter-propagate on the metallic waveguide like the SPPs, with identical wavevector magnitude.

The NSOM system employed in this work can perform measurements as a function of the tip-to-surface distance, thus experimentally reproducing the simulation conditions. Figure 5c presents such measurement, which is in excellent agreement with theory. It is even possible to qualitatively distinguish the presence of the QC waves that extend up to several micrometers from the surface. The maximum of the intensity at the metal–air interface provides evidence of the SPP presence.

Conclusions. We have developed and demonstrated a semiconductor-based technique for SPP generation by electrical injection. We believe that this integrated approach is promising for the development of SPP amplifiers too. The fundamental study of the metal proximity to a gain medium, combined with the electrical injection, opens the way to the development of electrically pumped semiconductor spasers (surface plasmon amplification by stimulated emission of radiation).[25]

AUTHOR INFORMATION

Corresponding Author

*E-mail: yannick.dewilde@espci.fr (Y.D.W.); raffaele.colombelli@u-psud.fr (R.C.).

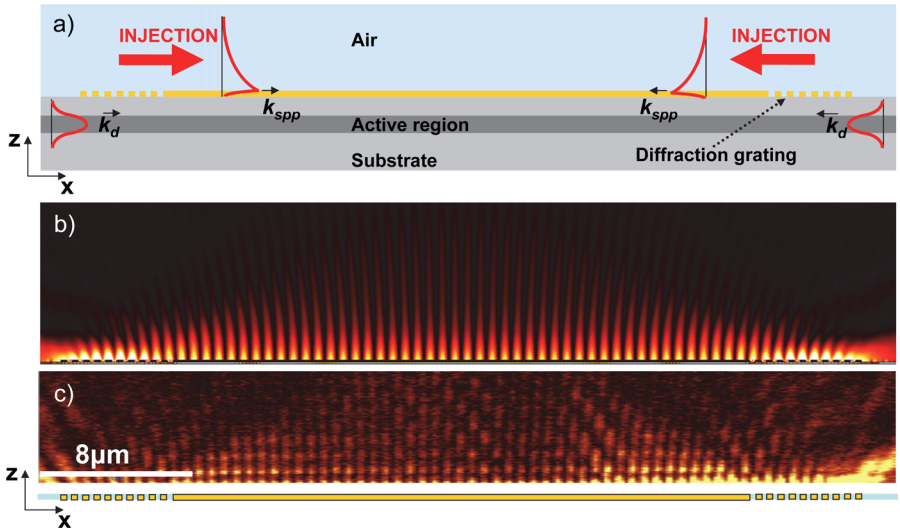

Figure 5. (a) Schematic side view of the device. Details about the active region and the semiconductor heterostructure can be found in ref 15. The red curves schematically represent the mode profiles of waveguided SPP modes. (b) Color-plot of the calculated squared modulus of the electric field in the $x-z$ plane (SPP interference pattern). (c) NSOM measurement in the $x-z$ plane, i.e., NSOM signal as a function of the tip-to-surface distance at several x-positions on the sample. The measurement qualitatively agrees with the simulation in panel b. The vertical intensity modulation is a perturbation due to interference between light directly transmitted through the nanohole and light scattered by the pyramid apex and back-reflected on the device surface into the nanohole.

dx.doi.org/10.1021/nl302040e | Nano Lett. 2012, 12, 4693–4697

Notes

The authors declare no competing financial interest.

■ ACKNOWLEDGMENTS

We thank B. Dagens, M. Fevrier, and J.-J. Greffet for useful discussions. The device fabrication has been performed at the nanocenter CTU-IEF-Minerve. This work was supported by the French National Research Agency (ANR-09-NANO-020 "GOSPEL") and the Triangle de la Physique (Project "PHLARE").

■ REFERENCES

(1) Ebbesen, T. W.; Genet, C.; Bozhevolnyi, S. I. Surface plasmon circuitry. *Phys. Today* **2008**, *61* (5), 44.
(2) Gramotnev, D.; Bozhevolnyi, S. I. Plasmonics beyond the diffraction limit. *Nat. Photonics* **2010**, *4*, 83.
(3) Berini, P.; De Leon, I. Surface plasmon−polariton amplifiers and lasers. *Nat. Photonics* **2012**, *6*, 16−24.
(4) Koller, D. M.; Hohenau, A.; Ditlbacher, H.; Galler, N.; Reil, F.; Aussenegg, F. R.; Leitner, A.; List, E. J.W.; Krenn, J. R. Organic plasmon-emitting diode. *Nat. Photonics* **2008**, *2*, 684.
(5) Ditlbacher, H.; Galler, N.; Koller, D. M.; Hohenau, A.; Leitner, A.; Aussenegg, F. R.; Krenn, J. R. Coupling dielectric waveguide modes to surface plasmon polaritons. *Opt. Express* **2008**, *16* (14), 10455−10464.
(6) Park, S. Y.; Kim, J. T.; Shin, J. S.; Shin, S. Y. Hybrid vertical directional coupling between a long range surface plasmon polariton waveguide and a dielectric waveguide. *Opt. Commun.* **2009**, *282* (23), 4513−4517.
(7) Hill, M. T.; Marell, M.; Leong, E. S.; Smalbrugge, B.; Ning, C.-Z. Lasing in metal-insulator-metal sub-wavelength plasmonic waveguides. *Opt. Express* **2009**, *17* (13), 11107.
(8) Kwon, S.-H.; Kang, J.-H.; Seassal, C.; Kim, S.-K.; Regreny, P.; Lee, Y.-H.; Lieber, C. M.; Park, H.-G. Subwavelength Plasmonic Lasing from a semiconductor nanodisk with silver nanopan cavity. *Nano Lett.* **2010**, *10*, 3679.
(9) Fedyanin, D. Y.; Krasavin, A. V.; Arsenin, A. V.; Zayats, A. V. Surface Plasmon Polariton Amplification upon Electrical Injection in Highly Integrated Plasmonic Circuits. *Nano Lett.* **2012**, *12* (5), 2459−2463.
(10) Grandidier, J.; Colas des Francs, G.; Massenot, S.; Bouhelier, A.; Markey, L.; Weeber, J.-C.; Finot, C.; Dereux, A. Gain-Assisted Propagation in a Plasmonic Waveguide at Telecom Wavelength. *Nano Lett.* **2009**, *9* (8), 2935−2939.
(11) Tetienne, J.-P.; Bousseksou, A.; Costantini, D.; Colombelli, R.; Babuty, A.; Moldovan-Doyen, I.; De Wilde, Y.; Sirtori, C.; Beaudoin, G.; Largeau, L.; Mauguin, O.; Sagnes, I. Injection of midinfrared surface plasmon polaritons with an integrated device. *Appl. Phys. Lett.* **2010**, *97*, 211110.
(12) Kim, C. S.; Vurgaftman, I.; Flynn, R. A.; Kim, M.; Lindle, J. R.; Bewley, W. W.; Bussmann, K.; Meyer, J. R.; Long, J. P. An integrated surface-plasmon source. *Opt. Express* **2010**, *18* (10), 10610.
(13) Aigouy, L; Lalanne, P.; Hugonin, J. P.; Julie, G.; Mathet, V.; Mortier, M. Near-Field Analysis of Surface Waves Launched at Nanoslit Apertures. *Phys. Rev. Lett.* **2007**, *98*, 153902.
(14) Decobert, J.; Lagay, N.; Cuisin, C.; Dagens, B.; Thedrez, B.; Laruelle, F. MOVPE growth of AlGaInAs−InP highly tensile-strained MQWs for 1.3 mm low threshold lasers. *J. Cryst. Growth* **2004**, *272*, 543.
(15) Costantini, D.; Bousseksou, A.; Fevrier, M.; Dagens, B.; Colombelli, R. Loss and gain measurements of tensile-strained quantum well diode lasers for plasmonic devices at telecom wavelengths. *IEEE J. Quantum Electron.* **2012**, *48*, 73.
(16) Babuty, A; Bousseksou, A.; Tetienne, J.-P.; Moldovan Doyen, I.; Sirtori, C.; Beaudoin, G.; Sagnes, I.; De Wilde, Y.; Colombelli, R. Semiconductor Surface Plasmon Sources. *Phys. Rev. Lett.* **2010**, *104*, 226806.
(17) Bousseksou, A.; Colombelli, R.; Babuty, A.; De Wilde, Y.; Chassagneux, Y.; Sirtori, C.; Patriarche, G.; Beaudoin, G.; Sagnes, I. A semiconductor laser device for the generation of surface-plasmons upon electrical injection. *Opt. Express* **2009**, *17* (11), 9391−9400.
(18) Tetienne, J.-P.; Bousseksou, A.; Costantini, D.; De Wilde, Y.; Colombelli, R. Design of an integrated coupler for the electrical generation of surface plasmon polaritons. *Opt. Express* **2011**, *19* (19), 18155−18163.
(19) Greusard, L.; Costantini, D.; et al. Unpublished.
(20) Witec: www.witec.de.
(21) Zia, R.; Schuller, J. A.; Brongersma, M. L. Near-field characterization of guided polariton propagation and cutoff in surface plasmon waveguides. *Phys. Rev. B* **2006**, *74*, 165415.
(22) Zia, R.; Brongersma, M. L. Surface plasmon polariton analogue to Young's double-slit experiment. *Nat. Nanotechnol.* **2007**, *2*, 426.
(23) Lalanne, P.; Hugonin, J. P.; Liu, H. T.; Wang, B. A microscopic view of the electromagnetic properties of sub- λ metallic surfaces. *Surf. Sci. Rep.* **2009**, *64*, 453−469.
(24) Comsol Multyphysics: www.comsol.com.
(25) Zheludev, N. I.; Prosvirnin, S. L.; Papasimakis, N.; Fedotov, V. A. Lasing Spaser. *Nat. Photonics* **2008**, *2*, 351.